ELECTRONIC SUPPORTING INFORMATION

2D self-assembly of o-OPE foldamers for chiroptical barcode

Irene López-Sicilia,[a] Ana M. Ortuño,*[b] Pablo Reine,[b] Darío Otero,[b] María T. Martín-Romero,[a] Luis Camacho,[a] Luis Álvarez de Cienfuegos,[b] Ángel Orte,[c] Juan J. Giner-Casares,*[a] Delia Miguel,*[c] and Juan M. Cuerva*[b]

a. *M. Sc. Irene López-Sicilia, Prof. María T. Martín-Romero, Prof. Luis Camacho, Prof. Juan J. Giner-Casares*

Departamento de Química Física
Universidad de Córdoba (UCO)
E-mail: jjginer@uco.es

b. *Dr. Ana M. Ortuño, Dr. Pablo Reiné, Darío Otero, Prof. Luis Álvarez de Cienfuegos, Prof. Juan M. Cuerva*

Departamento de Química Orgánica, Facultad de Ciencias, C. U. Fuentenueva
Universidad de Granada (UGR), Unidad de Excelencia de Química Aplicada a la Biomedicina y Medioambiente (UEQ)
E-mail: jmcuerva@ugr.es

c. *Prof. Ángel Orte, Prof. Delia Miguel*

Departamento de Fisicoquímica, Facultad de Farmacia, C. U. Cartuja
Universidad de Granada (UGR), (UEQ)
E-mail: dmalvarez@ugr.es

Table of Contents

1. SYNTHETIC PART

General Details

The following palladium catalysts, trans-dichlorobis(triphenylphosphine) palladium(II) ($Pd(PPh_3)_2Cl_2$) and trans-dichlorobis(acetonitrile)palladium(II) ($Pd(CH_3CN)_2Cl_2$), were prepared from palladium(II) chloride ($PdCl_2$) according to previously described procedures.[1] All reagents and solvents (CH_2Cl_2, EtOAc, Hexane, THF, *i*Pr_2NH, Et_3N, MeOH, CH_3CN) were purchased from standard chemical suppliers and used without further purification. Anhydrous THF was freshly distilled over Na/benzophenone. Thin-layer chromatography analysis was performed on aluminium-backed plates coated with silica gel 60 (230-240 mesh) with F_{254} indicator. The spots were visualized with UV light (254 nm and 360 nm) and/or stained with phosphomolybdic acid (10% ethanol solution) and subsequent heating. Column chromatography purifications were performed with silica gel 60 (40-63 μm). ^1H and ^{13}C NMR spectra were recorded on a Varian Direct Drive (500 MHz) or Bruker Avance Neo (400 MHz or 500 MHz) spectrometers at a constant temperature of 298 K. Chemical shifts are reported in ppm using residual solvent peak as reference ($CDCl_3$: δ = 7.26 ppm). Data are reported as follows: chemical shift, multiplicity (s: singlet, d: doublet, t: triplet, q: quartet, quint: quintuplet, hept: heptuplet, m: multiplet, dd: doublet of doublets, dt: doublet of triplets, td: triplet of doublets, bs: broad singlet), coupling constant (J in Hz) and integration; ^{13}C NMR spectra were recorded at 101 or 126 MHz using broadband proton decoupling and chemical shifts are reported in ppm using residual solvent peaks as reference ($CDCl_3$: δ = 77.16 ppm). Carbon multiplicities were determined by DEPT techniques. High-resolution mass spectra (HRMS) were recorded using EI on a Micromass GCT Agilent Technologies 6890N (Waters), by APCI mass spectra carried out on a Bruker MAXIS II mass spectrometer or by ESI mass spectrometry carried out on a Waters Xevo G2-XS QTof mass spectrometer. The following known compounds were isolated as pure samples and showed NMR spectra identical to reported data: **1**, **3**, **4**.[2]

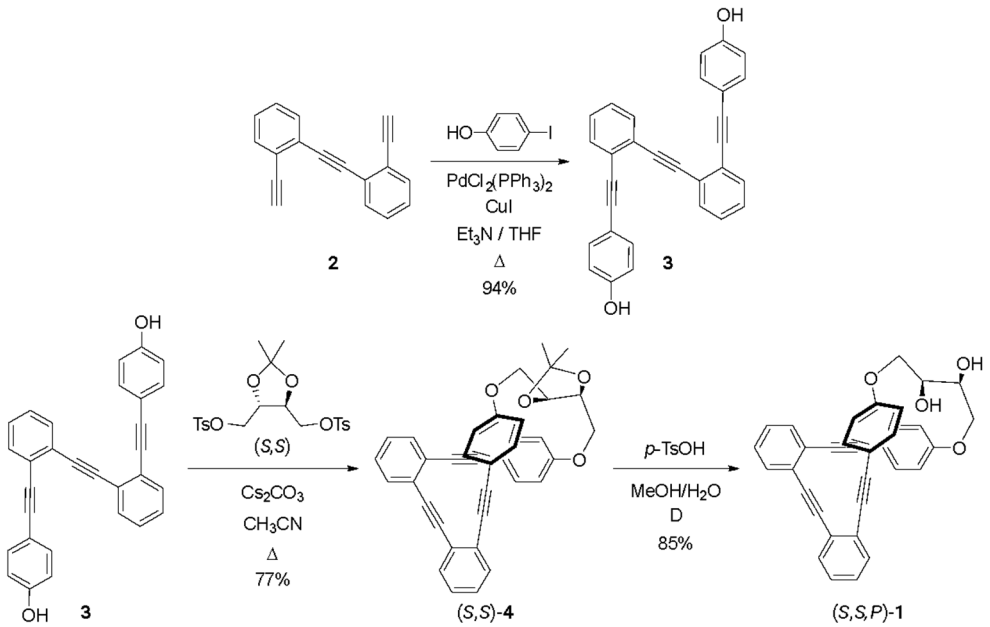

Scheme S1. Synthesis of compound (*S*,*S*,*P*)-**1**.

2. TRANSFERENCE OF FILMS FROM AIR/WATER INTERFACE

General Details

Dichloromethane (≥ 99.8%) was purchased from Sigma-Aldrich and was used as the spreading solvent without further purification. The concentration of spread molecule in dichloromethane was 1mM. Ultrapure water used as the subphase produced by a Millipore Milli-Q unit and pre-treated by a Millipore reverse osmosis system (>18.2 MΩ·cm^{-1}). The subphase temperature was 21ºC. All experiments were performed on tables with vibration isolation using the antivibration system MOD-2 S (Accurion, Göttingen, Germany) in a large class 1000 clean room.

- Transference of films from air/water interface. The multilayers were transferred onto quartz substrates by sequential Langmuir-Schaefer (LS) or Langmuir-Blodgett procedures. For Langmuir-Schaefer, i. e., horizontal dipping at constant surface pressure (π = 15 mN/m) was used. For Langmuir–Blodgett method, i.e., vertical dipping at constant surface pressure was used at a lifting speed of 5 mm·min^{-1}. The transfer pressure was kept at 15 mN/m. In the transfer process, only the monolayer is deposited during withdrawal of the substrate through the interface, giving rise to LB film type Z. The transfer ratio is close to unity and zero for the withdrawal and immersion processes, respectively. Multilayers on solid substrates were assembled by sequential monolayer transfer. The transfer ratio was closed to unity for all transferences. The solid

substrates were cleaned with an alkaline detergent, ethanol and isopropanol and then rinsed several times with ultrapure water.

- Surface pressure–area isotherms. Two different models of Nima troughs (Nima Technology, Coventry, England) were used in this work, both provided with a Wilhelmy type dynamometric system using a strip of filter paper: a NIMA 611D with one moving barrier for the measurement of the reflection spectra, and a NIMA 601, equipped with two symmetrical barriers to record BAM images. To spread the amphiphilic molecule solutions on the balances, Hamilton syringes were used. After spreading the compounds, 15 minutes were allowed before starting compression to ensure complete evaporation of the dichloromethane. The films were compressed at a speed of 0.02 $nm^2 \cdot min^{-1} \cdot molecule^{-1}$ (Figure S1).

- UV-vis reflection spectroscopy. UV-visible reflection spectra at normal incidence as the difference in reflectivity (ΔR) of the film-covered water surface and the bare surface were obtained with a Nanofilm Surface Analysis Spectrometer (Ref SPEC^2, supplied by Accurion GmbH, Göttingen, Germany).

- Brewster angle microscopy. Images of the film morphology were obtained by Brewster angle microscopy (BAM) with a I-Elli2000 (Accurion GmbH) using a Nd:YAG diode laser with wavelength 532 nm and 50 mW, which can be recorded with a lateral resolution of 2 μm. The image processing procedure included a geometrical correction of the image, as well as a filtering operation to reduce interference fringes and noise (Figures S2 and S3).

UV-vis spectra of bulk solutions and solid substrates were measured using a Cary 100 UV-Vis spectrophotometer.

- Molecular dynamics (MD) simulations. They were performed to gain further insights on the self-assembly process. The XYZ dimension values of the computational box were 24 x 30 x 150 $Å^3$. A bilayer with 32 (*S*,*S*,*P*)-**1** or (*R*,*R*,*M*)-**1** molecules (16 in each layer) was placed in said box. The periodic box was completed with water molecules maintaining the density of 1 g/cm^3. The low energy structures was explored using the Forcite Anneal task available in the Forcite plus module implemented in BIOVIA Materials Studio 2020.[3] The Forcite Anneal task consisted on a number of cycles of dynamics runs for which the temperature was changed gradually from 300 to 500 K and then decreased again to the initial temperature. A total of 20 annealing cycles were performed with structure minimization after each cycle. Data analysis was performed with the final structure after each cycle. For all calculations, the Dreading forcefield was used and the charge was assigned using Gasteiger.[4]

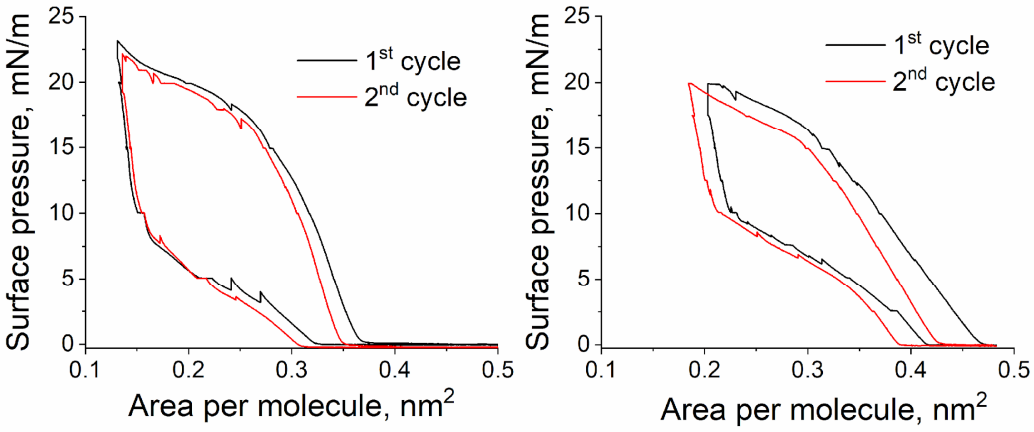

Figure S1. Surface pressure-molecular area isotherms and compression-expansion cycles for (*S*,*S*,*P*)-**1** (left) and (*R*,*R*,*M*)-**1** (right). Cycles as noted in the inset.

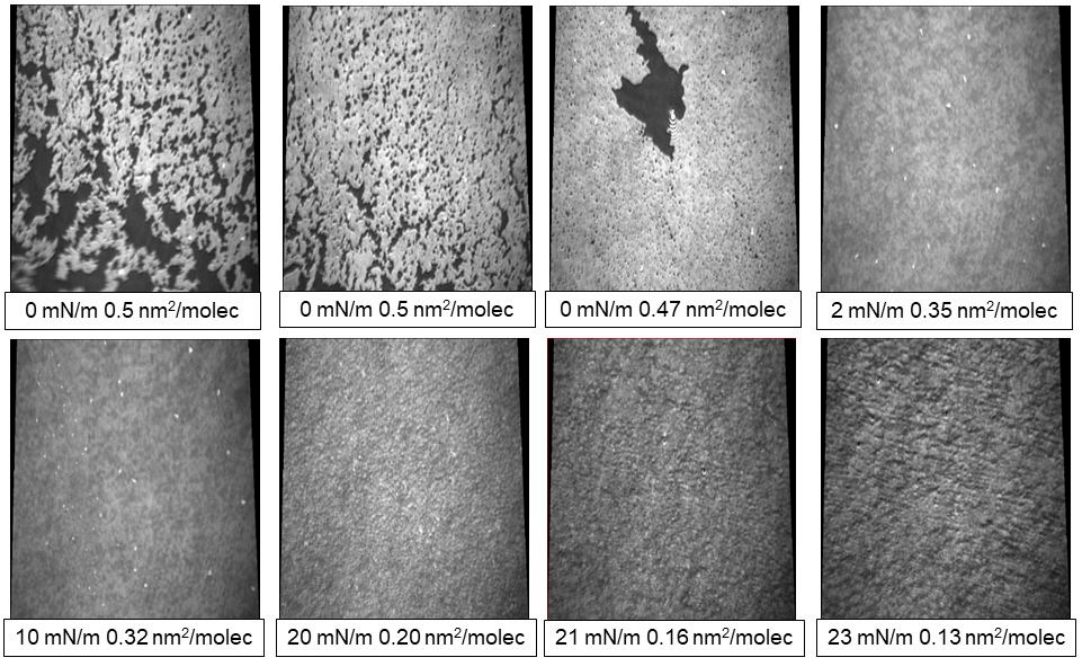

Figure S2. Brewster Angle Microscopy (BAM) pictures of (*S*,*S*,*P*)-**1** in situ at the air/water interface recorded during the first cycle of compression. The values of the surface pressure and area per molecule are noted in the insets. The width of each frame corresponds to 215 μm.

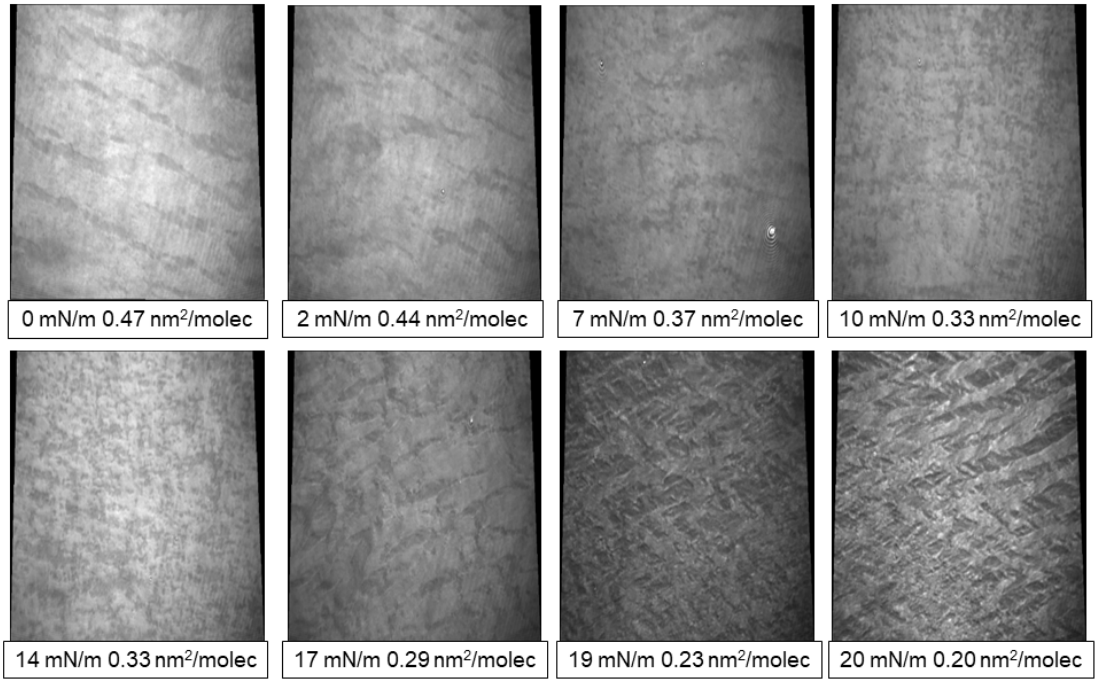

Figure S3. Brewster Angle Microscopy (BAM) pictures of (*R*,*R*,*M*)-**1** in situ at the air/water interface recorded during the first cycle of compression. The values of the surface pressure and area per molecule are noted in the insets. The width of each frame corresponds to 215 μm.

UV-Visible spectrum simulation and bands assignment

Computer simulations allowed obtaining the UV-vis spectrum of 2 as well as the orientation of the transition dipoles corresponding to the UV-vis bands. The geometry of the (*R*,*R*,*M*)-**1** molecule was previously optimized by using the AM1 semi-empirical method. A C_2 symmetry was imposed. In vacuo condition was set, using the ZINDO/S-CI semi-empirical method, with the Overlap Weighting Factor sigma-sigma = 1.267 and π-π = 0.51.[5] Note this semi-empirical method was purposefully designed to reproduce UV-vis spectra of organic molecules, offering a similar accuracy as DFT methods.[6] Both calculations were performed using the software Hyperchem 8.[7]

The transitions between the 8 occupied molecular orbitals of highest energy and 8 unoccupied molecular orbitals of lower energy were obtained. A total of 128 possible transitions, 64 singlets (ΔS=0) and 64 triplets (ΔS=1) were analyzed. Of these transitions, only 5 display values of wavelength λ_{max} > 280 nm, and oscillator strength > 0.05, see Figure S4. These transitions correspond to the modes λ_1 - λ_5. Table S1 indicates the wavelength and oscillator strength of the mentioned modes as well as additional modes with lower intensity appearing for λ_{max} > 280 nm.

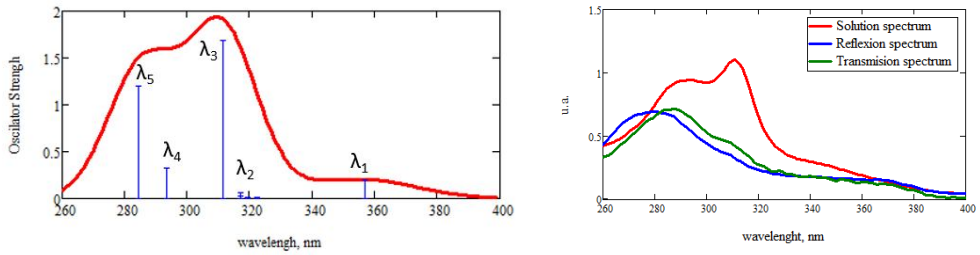

Figure S4. Left: *In vacuo* simulated UV-vis spectrum of (*R*,*R*,*M*)-**1**. Right: solution spectrum.

Table S1. Wavelength, oscillator strength and orientation of the different absorption modes from the *in vacuo* simulated UV-vis spectrum of (*R*,*R*,*M*)-**1**.

Transition	Wavelenght, nm	Oscillator strenght	Orientation axes
λ_1	356.9	0.196	x-y
--	322.2	0.012	z
--	319.4	0.011	x-y
--	317.2	0.019	x-y
λ_2	317.1	0.062	z
λ_3	311.3	1.688	z
λ_4	293.5	0.321	z
λ_5	284.1	1.197	x-y

The directions of the transition dipoles have been theoretically calculated for the different absorption components. The transition dipoles of λ_1 and λ_5 absorbing components are oriented along the x-y plane of the molecule, see Figure S5. On the other hand, the λ_2, λ_3 and λ_4 component is directed along the z axis, see Figure S5.

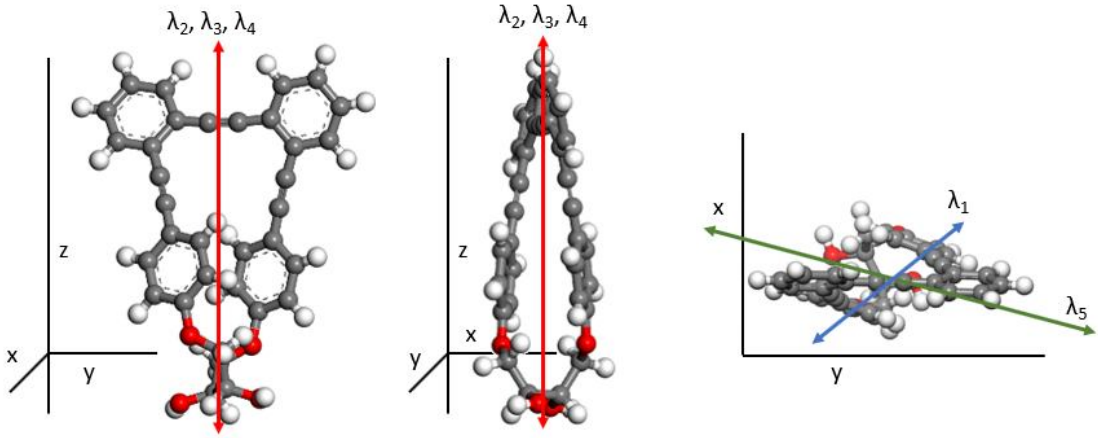

Figure S5. Transition dipole component orientation. Z axis corresponds to the perpendicular axis to the air/water interface plane.

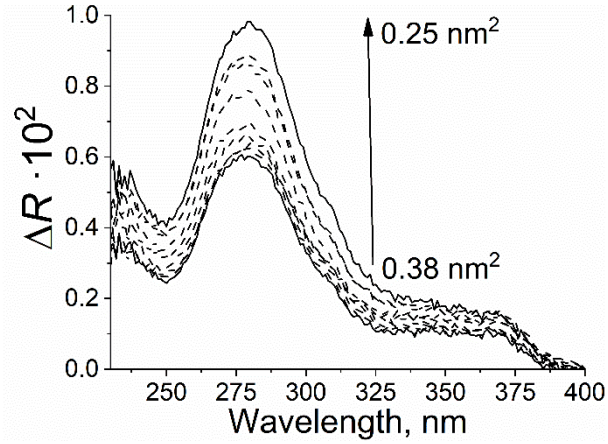

Figure S6. In situ UV-vis reflection spectra of (*R*,*R*,*M*)-**1** at the air/water interface. The area values per (*R*,*R*,*M*)-**1** molecule are noted in the inset.

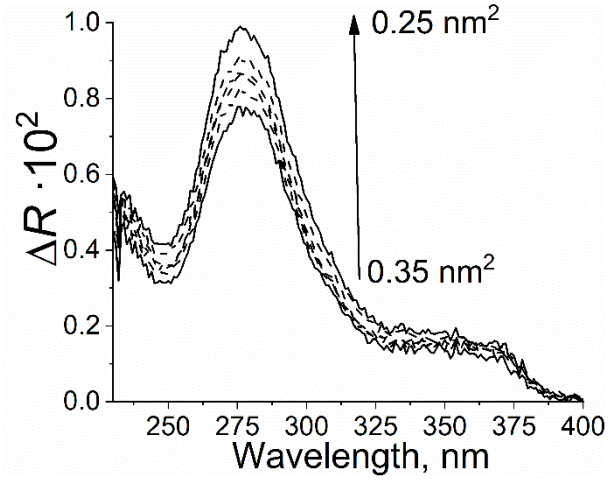

Figure S7. In situ UV-vis reflection spectra of (*S*,*S*,*P*)-**1** at the air/water interface. The area values per (*S*,*S*,*P*)-**1** molecule are noted in the inset.

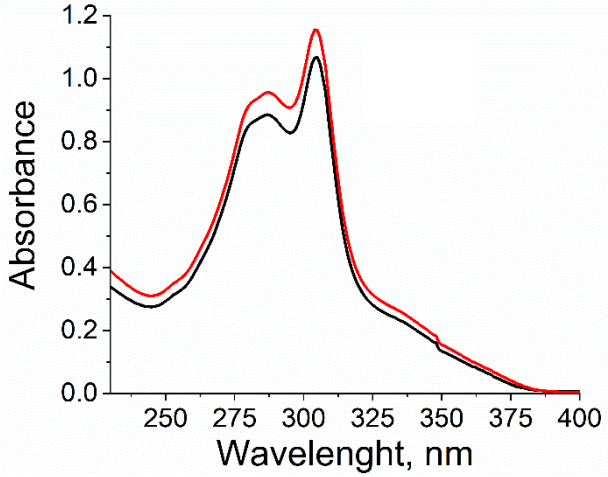

Figure S8. Transmission UV-vis spectra of (*S*,*S*,*P*)-**1** (black line) and (*R*,*R*,*M*)-**1** (red line) recorded in bulk solution, black and red line, respectively. Dichloromethane was used as a solvent.

Table S2: wavelength, oscillator strength and orientation of the different absorption modes from the *in vacuo* simulated UV-vis spectrum of (*R*,*R*,*M*)-**1**.

Type of H-bond	**(*S*,*S*,*P*)-1**	**(*R*,*R*,*M*)-1**
Intramolecular -OH to O(C)C-	18.1	29.6
Intermolecular -OH to O(C)C-	1.35	1.55
Intramolecular -OH to HO-	2.7	0.9
Intermolecular -OH to HO-	1.45	1.75
Total number of intramolecular H-bonds	20.8	30.5
Total number of intermolecular H-bonds	2.8	3.3
o-OPE foldamer to water: -OH to water	26.65	22.7
o-OPE foldamer to water: -HO to water	22.25	23.65
o-OPE foldamer to water: -CO to water	11.25	9.9
Total number of H-bonds with water	60.15	56.25
Total number of H-bonds	83.75	90.05
Total number of H-bonds per molecule	2.62	2.81

3. PHOTOPHYSICAL PROPERTIES

FLIM and anisotropy imaging was performed on an Abberior Expert Line instrument (Abberior GmbH), based on an Olympus IX83 confocal microscope. For FLIM imaging a pulsed 375-nm diode laser, working at 20 MHZ, was used as the excitation source, and the emitted fluorescence was detected on a hybrid PMT after a 509/22 bandpass filter. Photon time tagging for single photon counting was performed on a HydraHarp 300 counter (Picoquant GmbH). FLIM images were collected using a dwell time of 120 µs per pixel, and variable pixel resolution. Anisotropy imaging was performed in the same instrument but using a combination of motorized quarter-wave plate and half-wave plate in the 375-nm excitation pathway. This allows control of the polarization of the excitation beam to any coordinate in the Poincaré sphere. We employed linearly polarized light at 0° and 90°, as well as LCP and RCP light. The fluorescence emission was split onto the vertical and horizontal polarization components, using a polarization cube, and sent to two point detectors after identical 509/22 bandpass filters.

Pixelwise FLIM analysis was carried out in SymphoTime 64 (Picoquant) by fitting the fluorescence decay traces to a biexponential decay function after a 3x3 spatial binning. A short decay time of 0.3 ns was kept as a fixed parameter, accounting for highly quenched emitters and scattered light, whereas the long decay time was an adjustable parameter. FLIM images were reconstructed using the intensity-weighted average lifetime. The analysis of lifetime values from different samples of (*S*,*S*,*P*)-**1** and (*R*,*R*,*M*)-**1** transferred in several layers onto glass slides was performed particle-wise using home-coded scripts in Fiji (distribution of ImageJ)[8]. To select the different regions of liquid phase separation, containing the different enantiomers of diol **1**, an automated segmentation procedure was followed. First, the intensity images were thresholded using the automated *Li* algorithm; then, the selected regions were segmented by the *Watershed* function to separate and identify different regions in close contact and applying the *Analyze Particles* routine in Fiji. The identified particles as ROIs were used to read out in the average lifetime of each particle. All the results from ROIs identified in different images of the same sample were plotted together in a violin plot using Flourish.

Anisotropy imaging and population analysis was also performed in Fiji, to calculate the I_H/I_V ratios and the I_{LCP}-I_{RCP} difference and reconstruct the images on a pseudocolor scale. I_{LCP} and I_{RCP} were obtained as the sum of I_H and I_V for each hand of CP light excitation. An automated threshold selection (*MaxEntropy* algorithm) was applied to the matrix of I_H+I_V to select the ROIs, and the corresponding histograms were collected. Histograms from different images of the same

sample were added up together for the overall histogram and subsequently normalized. The histograms were fitted to Gaussian functions using OriginPro 9.0.

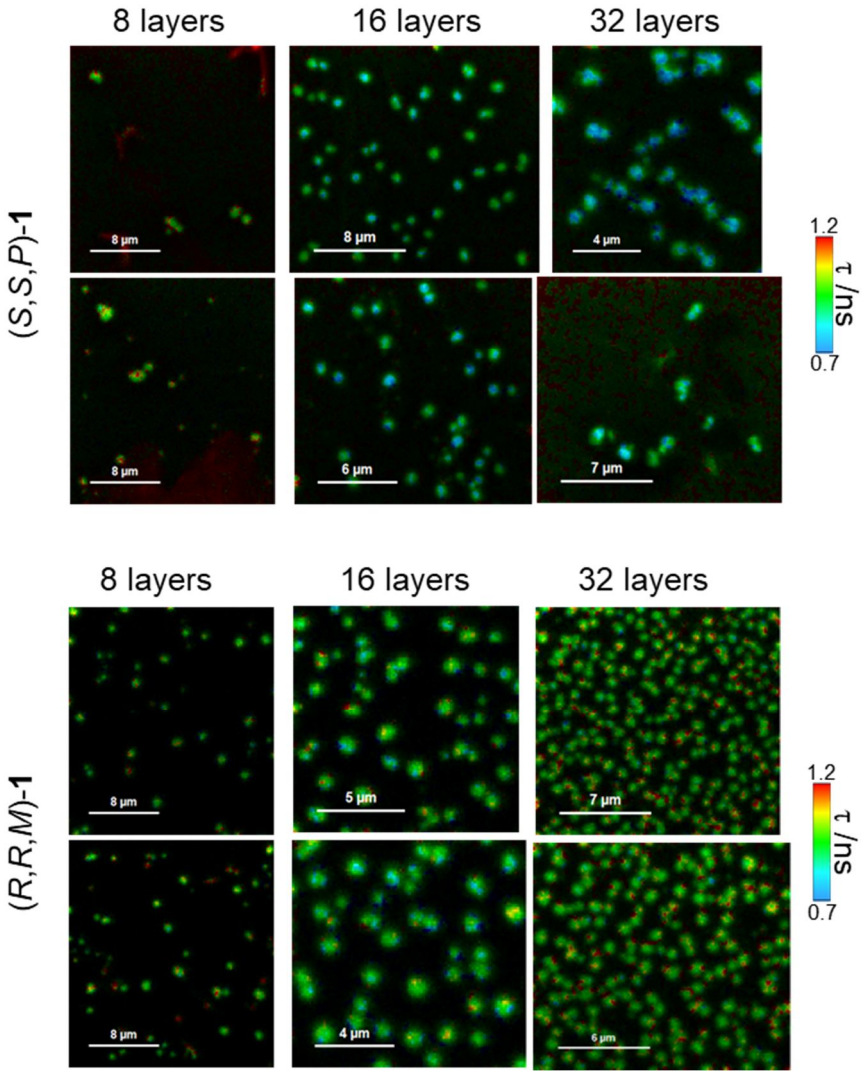

Figure S9. Additional examples of representative FLIM images of compounds (*S*,*S*,*P*)-**1** (upper panel) and (*R*,*R*,*M*)-**1** (lower panel) transferred onto glass slides after subsequent deposition of 8, 16, or 32 layers.

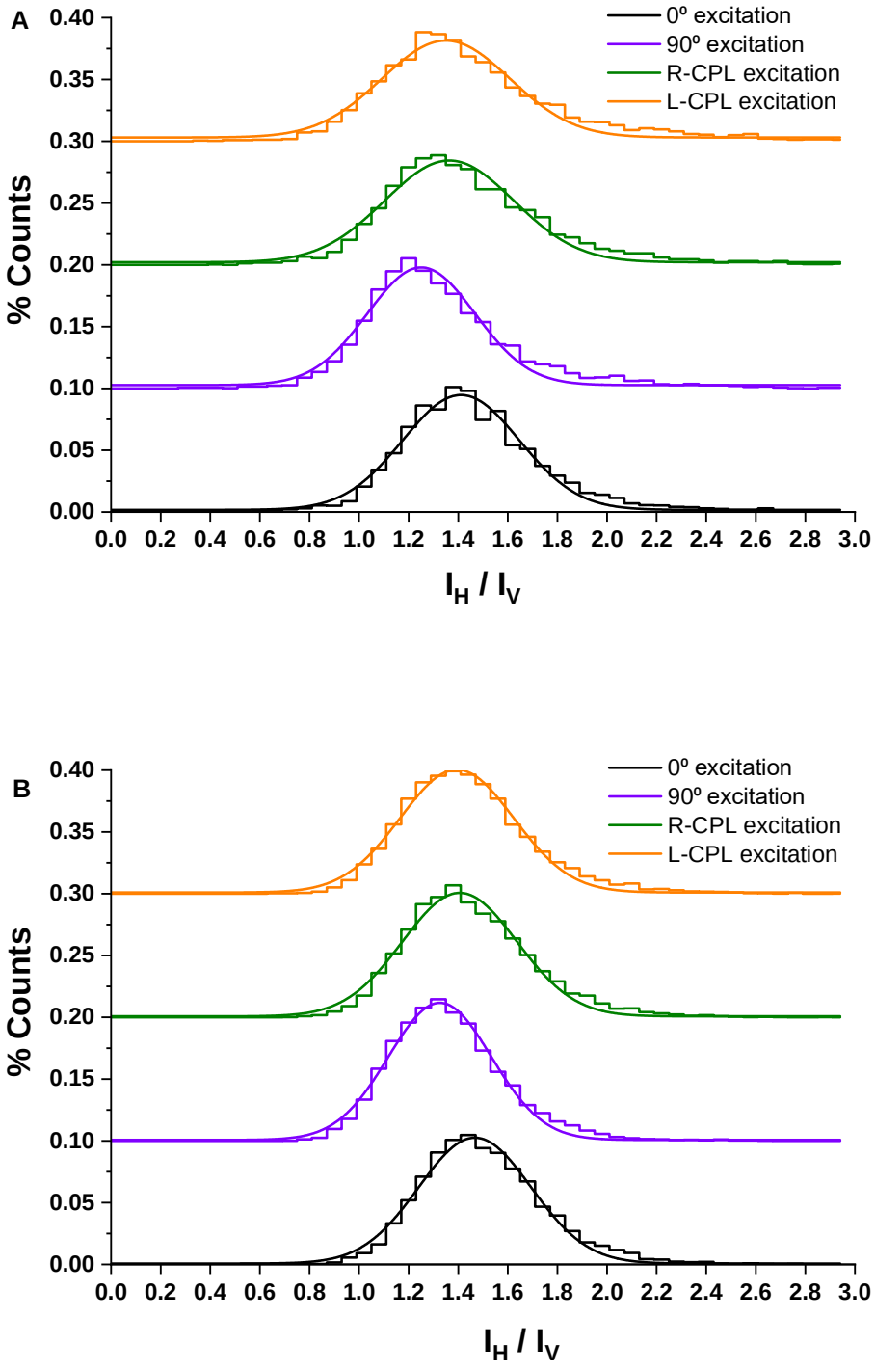

Figure S10. Extracted overall I_H/I_V ratio histograms (from, at least, 4 different images) of compound (*S,S,P*)-**1** transferred onto glass slides after subsequent deposition of (A) 8 layers and (B) 32 layers at different excitation polarizations.

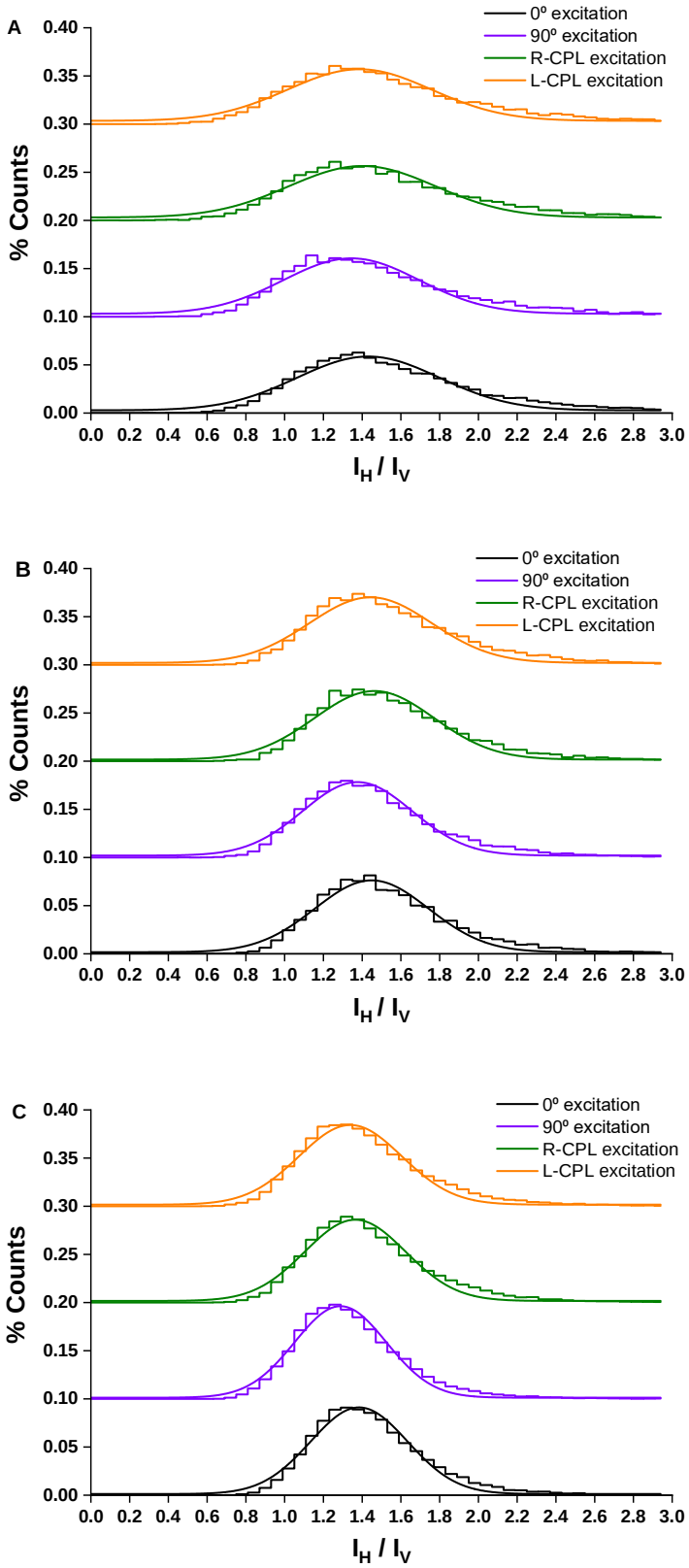

Figure S11. Extracted overall I_H/I_V ratio histograms (from, at least, 4 different images) of compound (*R,R,M*)-**1** transferred onto glass slides after subsequent deposition of (A) 8 layers, (B) 16 layers and (C) 32 layers at different excitation polarizations.

We have also compared the intensity of the signal using the same excitation but changing the number of monolayers of the sample (Figures S12-13). We noticed that the higher the number of monolayers the higher the intensity, although no direct relationship could be gathered.

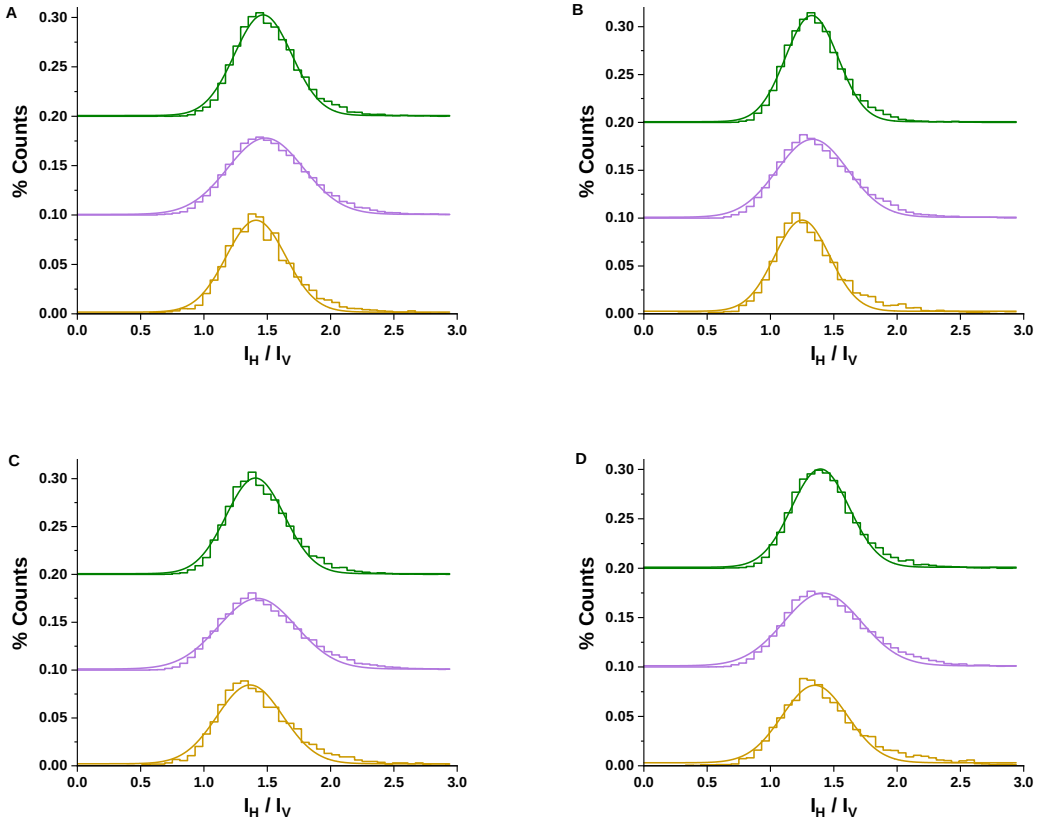

Figure S12. Extracted overall I_H/I_V ratio histograms (from, at least, 4 different images) of compound (*S,S,P*)-**1** transferred onto glass slides after subsequent deposition of 8 layers (dark yellow), 16 layers (violet) and 32 layers (olive green) at (A) 0^0, (B) 90^0, (C) R-CPL and (D)-L-CPL excitation polarizations.

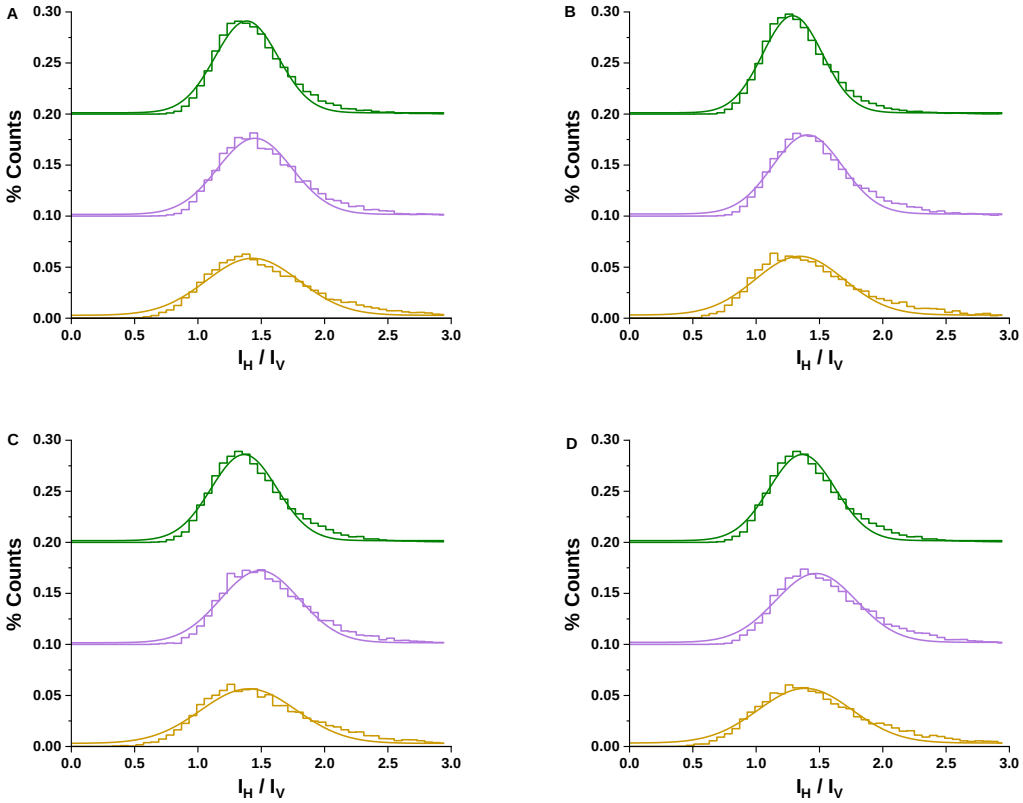

Figure S13. Extracted overall I_H/I_V ratio histograms (from, at least, 4 different images) of compound (*R,R,M*)-**1** transferred onto glass slides after subsequent deposition of 8 layers (dark yellow), 16 layers (violet) and 32 layers (olive green) at (A) 0^0, (B) 90^0, (C) R-CPL and (D)-L-CPL excitation polarizations.

In order to test whether we detected any polarization in the emitted light, we compared the histograms obtained by the difference of intensities when exciting with L-CPL (I_L) and R-CPL (I_R). Although we observed a deviation to negative values, it was obtained for both enantiomers (Figure S14), thus coming from the different sensitivity of the optical elements towards light with different polarization, instead of from the chiral selection of the sample.

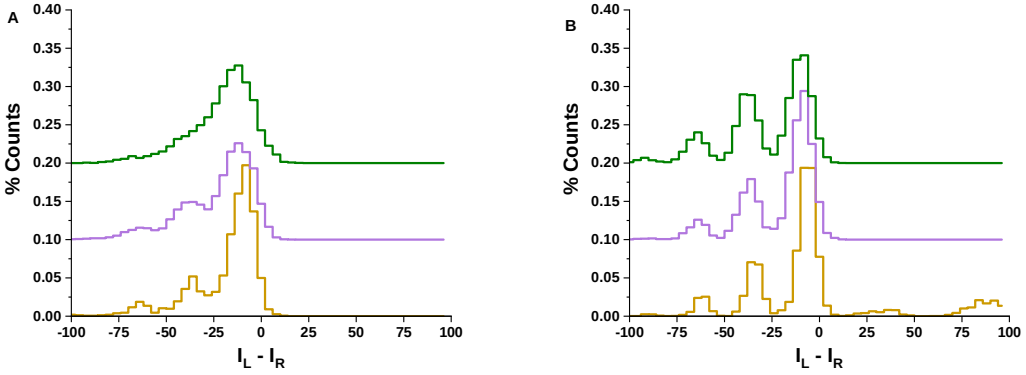

Figure S14. Extracted overall I_L- I_R histograms (from, at least, 4 different images) of compound (A) (*S,S,P*)-**1** and (B) (*R,R,M*)-**1** transferred onto glass slides after subsequent deposition of 8 layers (dark yellow), 16 layers (violet) and 32 layers (olive green) .

4. CHIROPTICAL PROPERTIES

Experimental Conditions

Both absorption and emission measurements were performed in an Olis DSM172 spectrophotometer. A xenon lamp of 150 W was used for absorption measurements, while to emission measurements fixed wavelength LED (250 nm) was used as the excitation source.

Chiroptical properties of (*S*,*S*,*P*)-**1** and (*R*,*R*,*M*)-**1** in solution were collected using a 1.0 cm path-length quartz cell and 2.5×10^{-5} M solutions with HPLC grade CH_2Cl_2. CD spectra were measured accumulating 30 scans. A fixed slit-width of 1 mm and 0.1s of integration time were selected. CPL spectra were collected by accumulating 150 scans with 0.5 s of integration time.

Chiroptical properties of (*S*,*S*,*P*)-**1** and (*R*,*R*,*M*)-**1** in solid state were collected using a 4.5x1.0x0.1 cm quartz plate with 1, 8, 16 and 32 monolayers (Langmuir-Schaefer films). In all these cases, in order to avoid linear dichroism (LD, Figure S21) and linear birefringence (LB),8 both CD and CPL spectra was measured in 8 different directions (θ=0°, 45°, 90°, 135°, 180°, 225°, 270°, 315°) (Scheme S2). The final results are the average of these measurements. Moreover, we checked there is no macroscopic anisotropy by measuring in "front" and "back" side of each quartz plate (Figure S22).[9] To CD spectra, a fixed slit-width of 1 mm and 0.1s of integration time were selected by accumulating 60 scans, whereas CPL spectra was collected by accumulating 300 scans with 1 s of integration time.

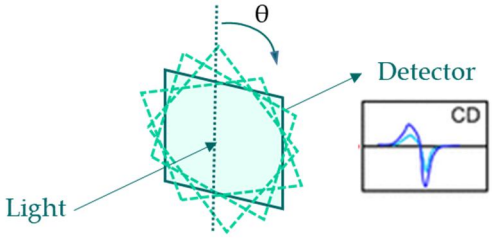

Scheme S2. Measurement methodology of CD and CPL spectra.

Absorbance and steady-state fluorescence spectra

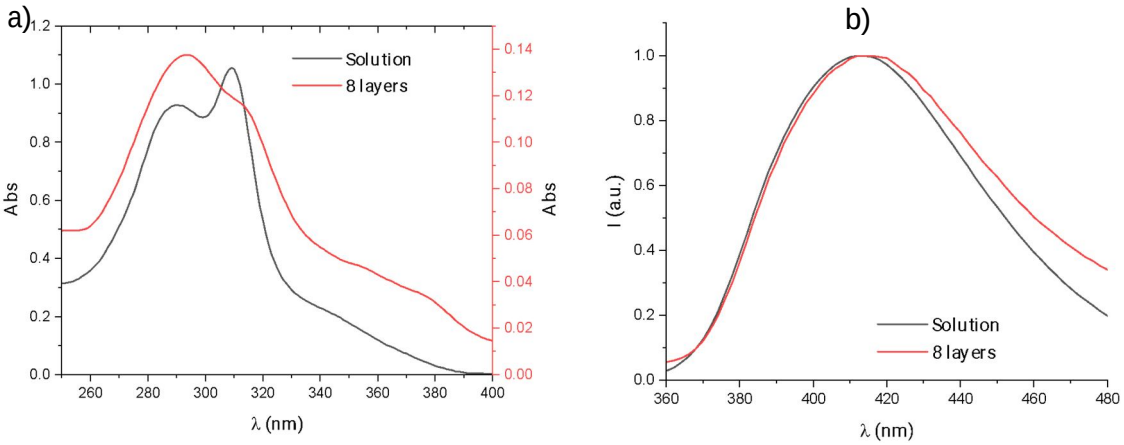

Figure S15. a) Absorption and b) fluorescence emission (λ_{exc} = 250 nm) spectra of compound (*S*,*S*,*P*)-**1** in CH_2Cl_2 (black line) and transferred onto a glass slide (red line).

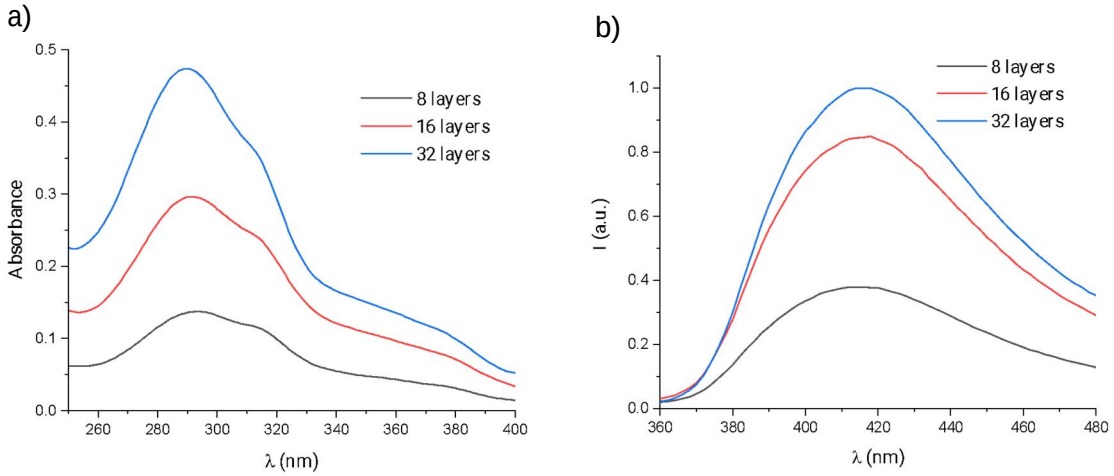

Figure S16. a) Absorption and b) fluorescence emission (λ_{exc} = 250 nm) spectra of compound (*S*,*S*,*P*)-**1** transferred onto a glass slide: 8 (black line), 16 (red line) and 32 (blue line) layers.

CD and CPL measurements

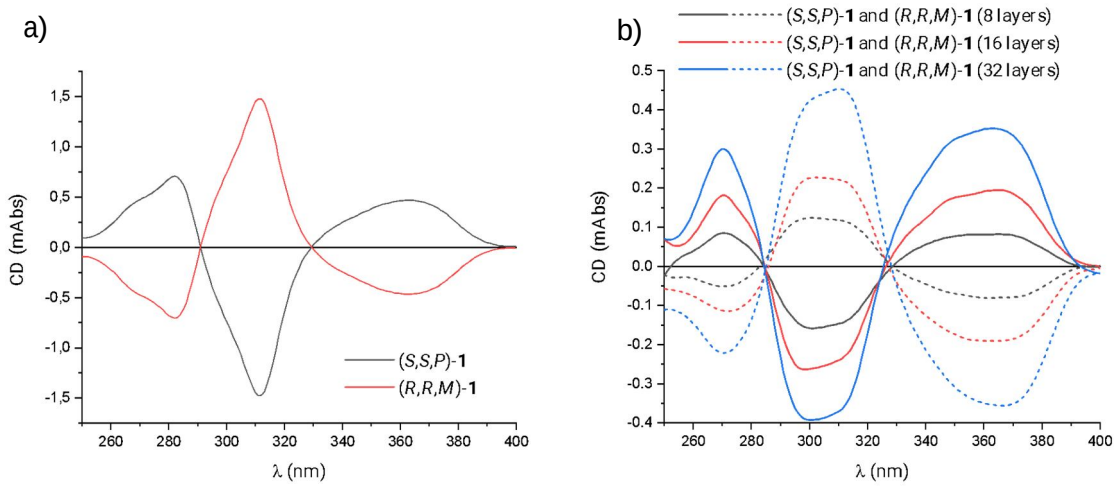

Figure S17. CD spectra of compounds (*S*,*S*,*P*)-**1** and (*R*,*R*,*M*)-**1** a) in CH_2Cl_2 and b) transferred onto a glass slide: 8 (black line), 16 (red line) and 32 (blue line) layers.

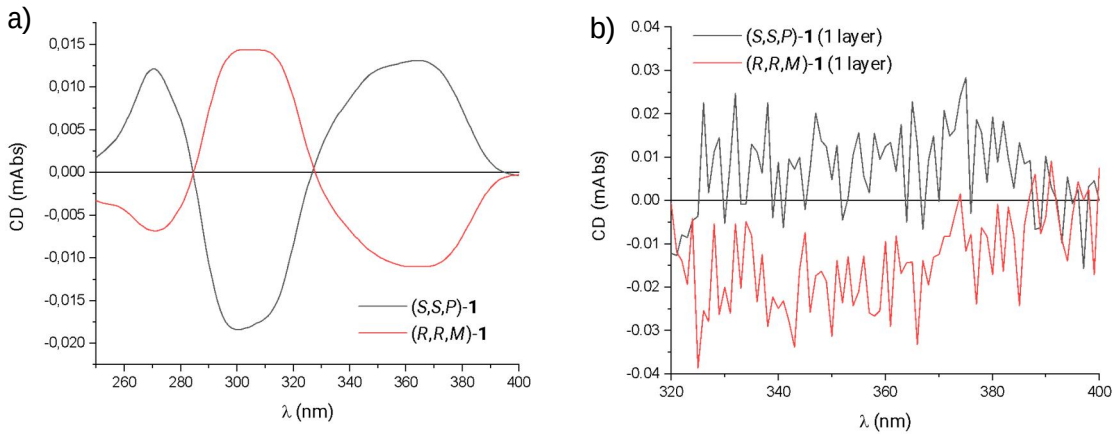

Figure S18. a) Predicted and b) experimental CD spectra of compounds (*S*,*S*,*P*)-**1** and (*R*,*R*,*M*)-**1** transferred onto a glass slide (1 layer).

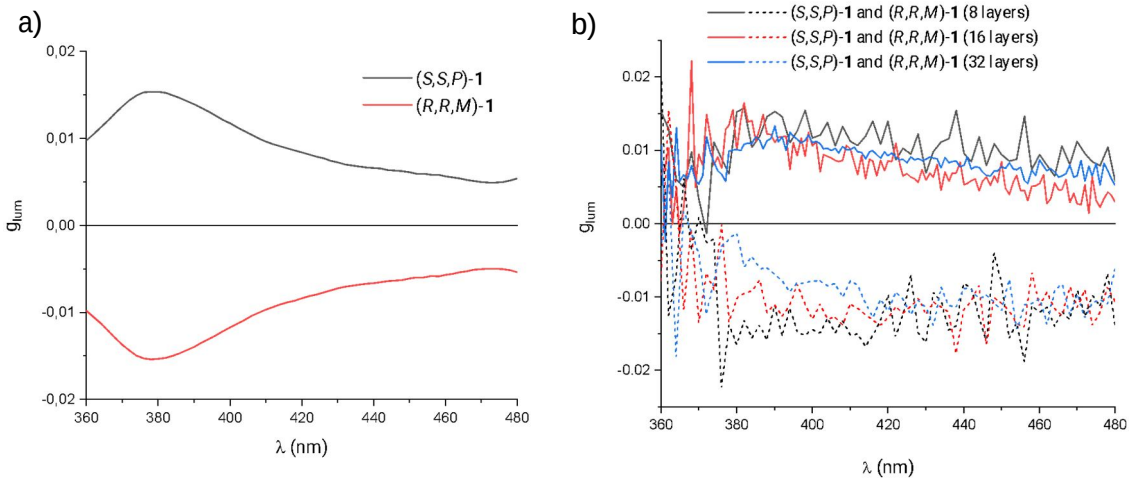

Figure S19. CPL spectra of compounds (*S*,*S*,*P*)-**1** and (*R*,*R*,*M*)-**1** a) in CH_2Cl_2 and b) transferred onto a glass slide: 8 (black line), 16 (red line) and 32 (blue line) layers.

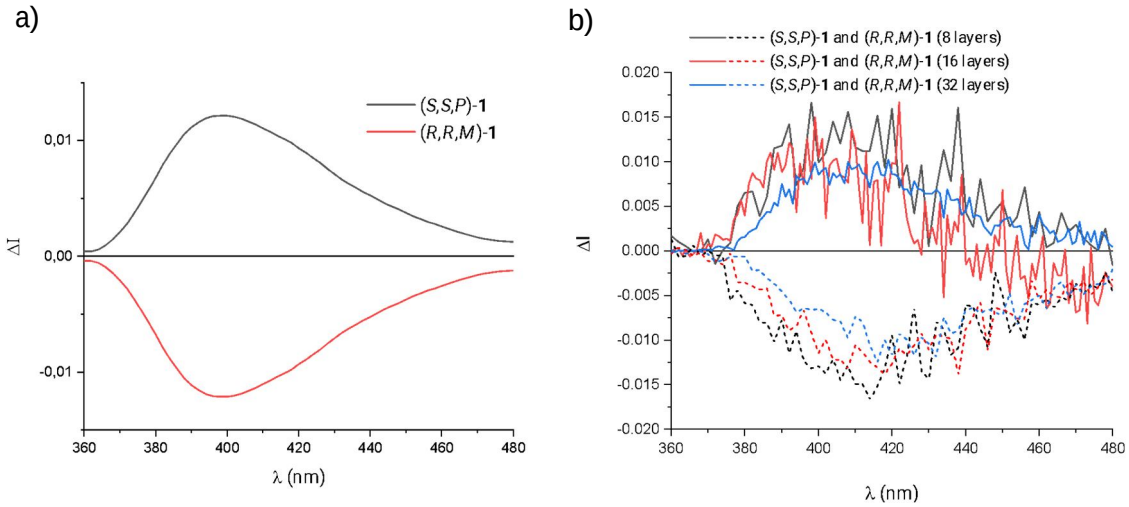

Figure S20. Normalized ΔI spectra of compounds (*S*,*S*,*P*)-**1** and (*R*,*R*,*M*)-**1** a) in CH_2Cl_2 and b) transferred onto a glass slide: 8 (black line), 16 (red line) and 32 (blue line) layers.

(*S*,*S*,*P*)-1	g_{abs}	g_{lum}
CH_2Cl_2	7.4×10^{-3} (381 nm)	1.2×10^{-2} (400 nm)
8 layers	2.1×10^{-3} (372 nm)	1.25×10^{-2} (407 nm)
16 layers	2.2×10^{-3} (371 nm)	1.0×10^{-2} (400 nm)
32 layers	2.9×10^{-3} (372 nm)	1.0×10^{-2} (405 nm)

Table S3. g_{abs} and g_{lum} values of (*S*,*S*,*P*)-**1** in different samples.

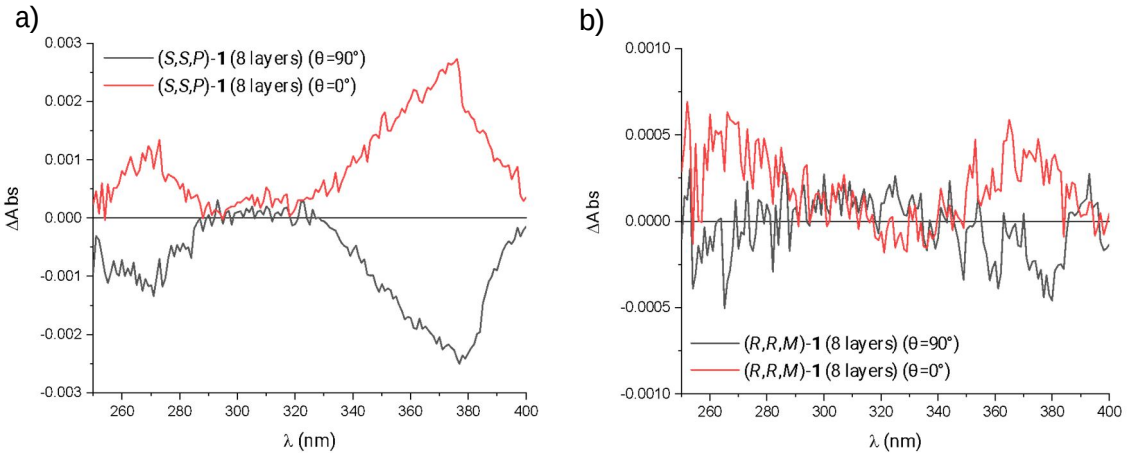

Figure S21. Linear dichroism spectra of compounds a) (*S*,*S*,*P*)-**1** and b) (*R*,*R*,*M*)-**1** in θ=0° and θ=90°.

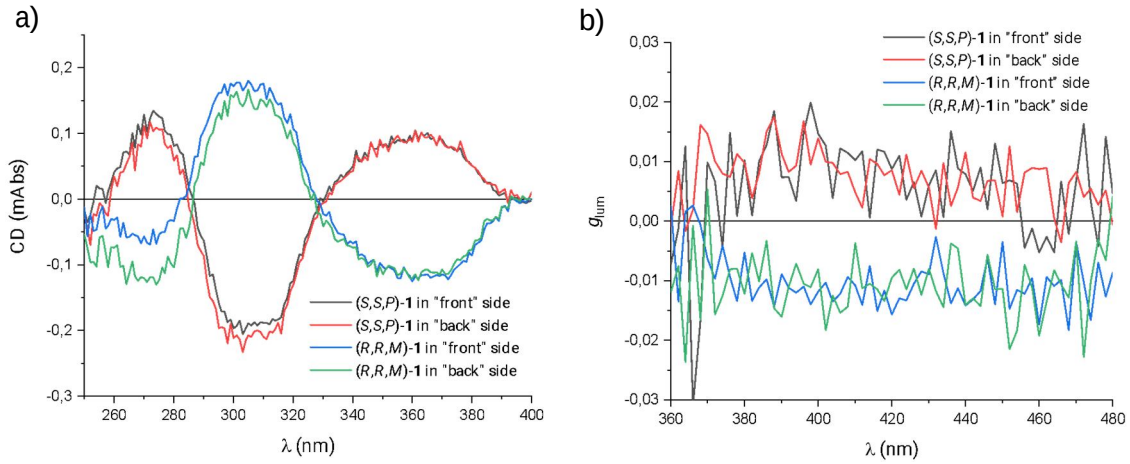

Figure S22. a) CD and b) CPL spectra of compounds (*S*,*S*,*P*)-**1** and (*R*,*R*,*M*)-**1** in "front" and "back" side.

Fast measurements in the maximum of CD and CPL spectra

Measurements were carried out in the same conditions just in a short-range corresponding to maximum intensity in CD and CPL spectra, by accumulating as few scans as possible to obtain reliable signals.

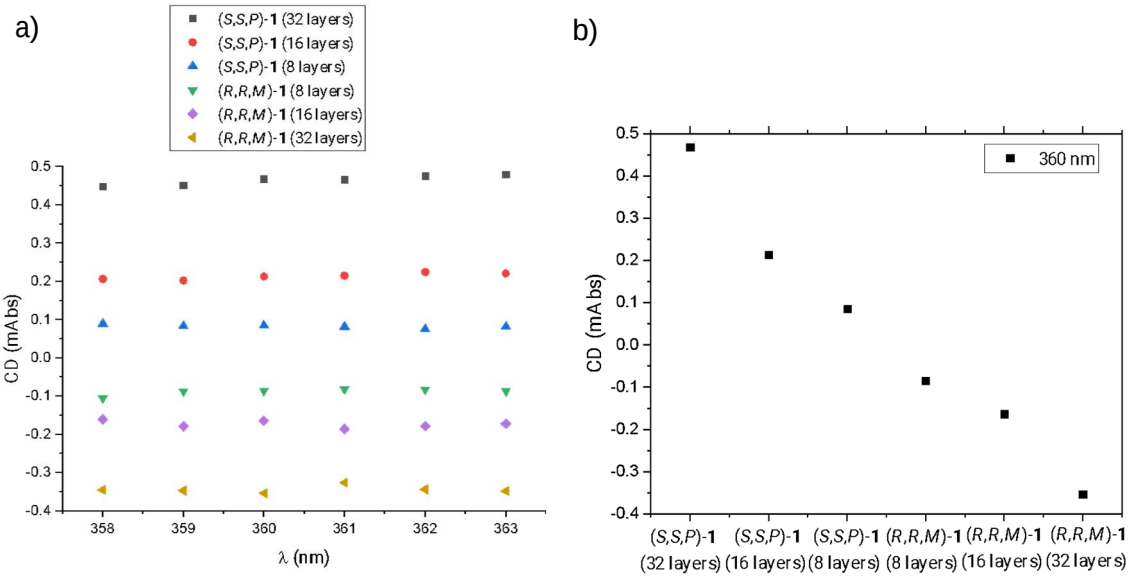

Figure S23. CD values of compounds (*S*,*S*,*P*)-**1** and (*R*,*R*,*M*)-**1** in a) a short range of the spectra and b) 360 nm. Measurement by accumulating 1 scan in each direction, 8 scans in total.

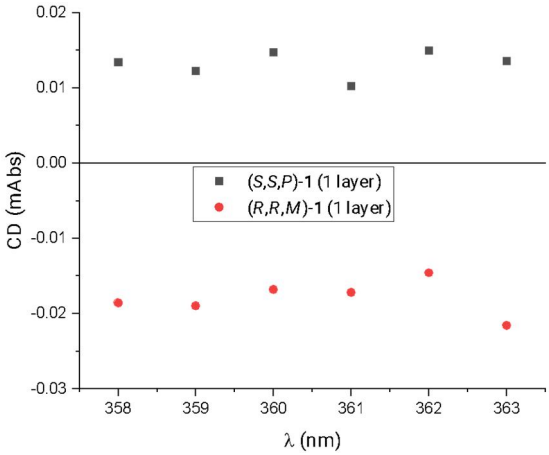

Figure S24. CD values of compounds (*S*,*S*,*P*)-**1** and (*R*,*R*,*M*)-**1** (1 layer) in a short range of the spectra. Measurement by accumulating 3 scan in each direction, 24 scans in total.

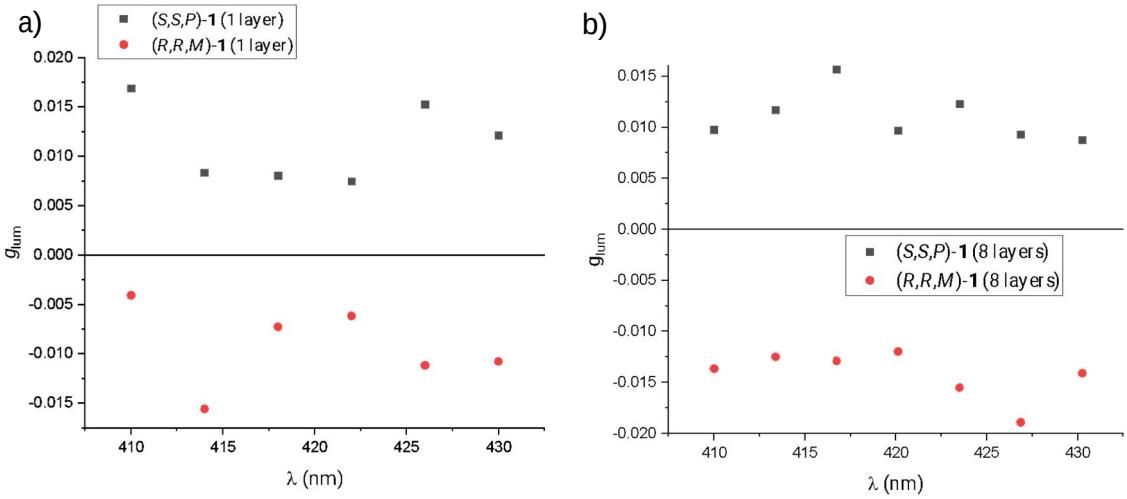

Figure S25. CPL values of compounds (*S*,*S*,*P*)-**1** and (*R*,*R*,*M*)-**1** in a short range of the spectra a) 1 layer and b) 8 layers. Measurement by accumulating 5 scans in each direction, 40 scans in total.

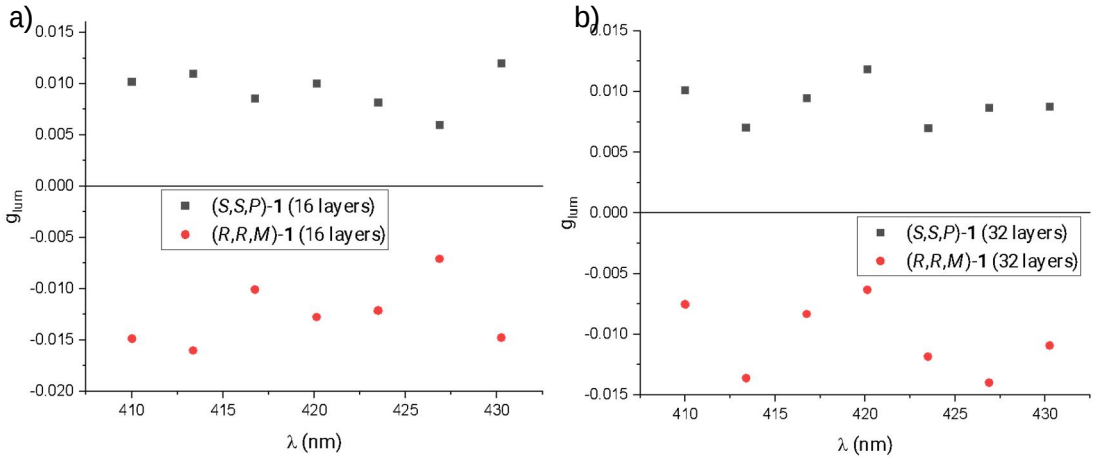

Figure S26. CPL values of compounds (*S*,*S*,*P*)-**1** and (*R*,*R*,*M*)-**1** in a short range of the spectra a) 16 layers and b) 32 layers. Measurement by accumulating 1 scan in each direction, 8 scans in total.

Reading of CD and CPL barcodes

Barcodes is based on two quartz plates with the same number of monolayers of (*S*,*S*,*P*)-**1** and (*R*,*R*,*M*)-**1** each one. In this way, two barcodes were measured: one of them with 16 monolayers and the other one with 32 monolayers. Both CD and CPL spectra were measured by accumulating 1 scan in each direction, 8 scans in total to read each band of barcode. In order to avoid macroscopic artefacts between both quartz plates, CD spectra were measured just in 2 points (Scheme S3a). However, due to 90° disposition of CPL equipment, CPL spectra were able to measure in 4 point (Scheme S3b).

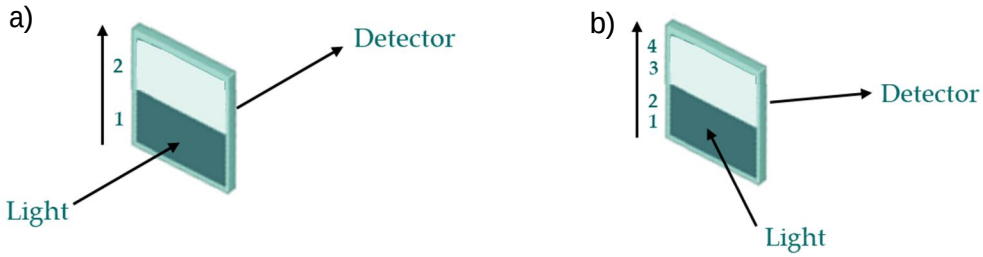

Scheme S3. Measurement methodology of a) CD and b) CPL spectra in barcodes.

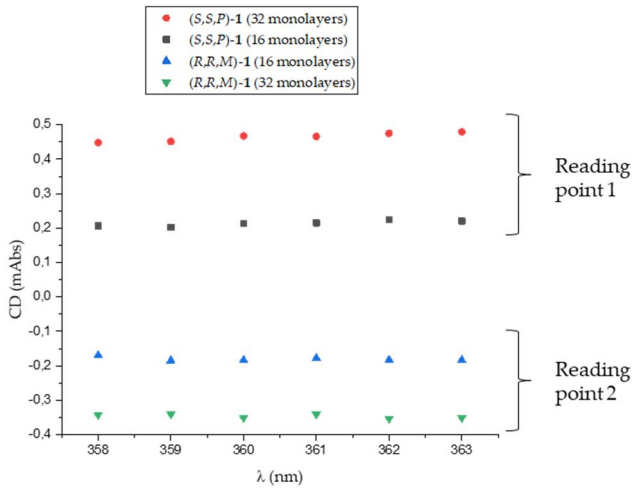

Figure S27. CD values of compounds (*S*,*S*,*P*)-**1** and (*R*,*R*,*M*)-**1** in barcodes: one with two bands of 16 layers (black and blue points), and another one with two bands of 32 layers (red and green points).

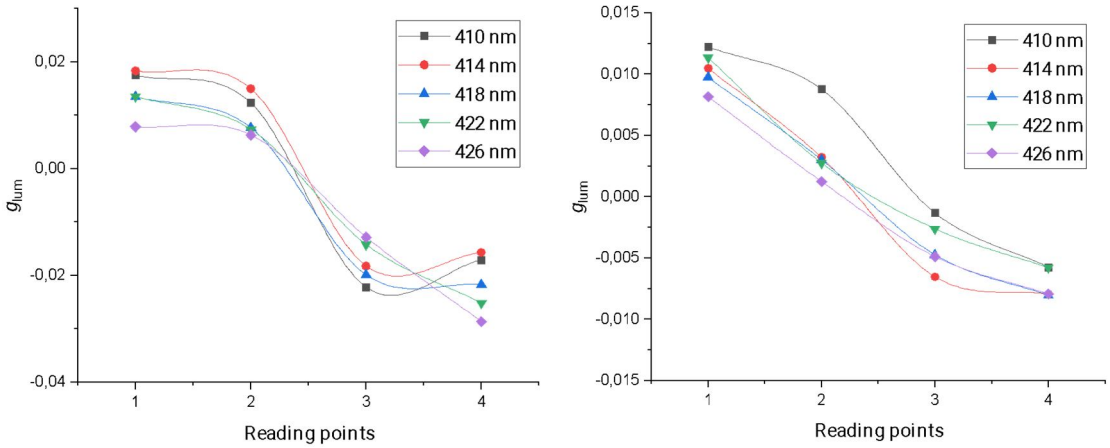

Figure S28. CPL values of compounds (*S*,*S*,*P*)-**1** and (*R*,*R*,*M*)-**1** in barcodes with a) two bands of 16 layers and b) two bands of 32 layers.

5. REFERENCES

[1] N. Miyaura, A. Suzuki, J. Chem. Soc., *Chem. Commun.*, 1979, 866.

[2] P. Reiné, J. Justicia, S. P. Morcillo, G. Mazzeo, E. García-Fernández, A. Rodríguez-Diéguez, L. Álvarez de Cienfuegos, S. Abbate, J. M. Cuerva, G. Longhi, D. Miguel, *Chirality*, 2018, **30**, 43–54.

[3] BIOVIA Materials Studio, 2020, Dassault Systémes

[4] J. Gasteiger and M. Marsili, *Tetrahedron*, 1980, **36**, 3219–3228.

[5] Neto, J. D. D.; Zerner, M. C. *Int. J. Quantum Chem*., 2001, **81**, 187.

[6] Safarpour, M. A.; Navir, S. B.; Jamali, M.; Mehdipour, A. R. *J. Mol. Struct*., 2009, **900**, 19.

[7] Hyperchem; 8th ed.; Htpercube, Inc.: Gainesville, FL, 2007.

[8]Schindelin, J.; Arganda-Carreras, I.; Frise, E.; Kaynig, V.; Longair, M.; Pietzsch, T.; Preibisch, S.; Rueden, C.; Saalfeld, S.; Schmid, B.; Tinevez, J.-Y.; White, D. J.; Hartenstein, V.; Eliceiri, K.; Tomancak, P.; Cardona, A., Nat. Meth., 2012, **9 (7)**, 676-682. DOI 10.1038/nmeth.2019.

[9] G. Albano, G. Pescitelli, L. Di Bari, *Chem. Rev.,* 2020, **120**, 10145-10243.